

Quaternary GaInAsSb 2.0-2.5 Micron Back-Illuminated Focal Plane Array for Blood Glucose Monitoring

J. P. Prineas^{a,b}, M. Reddy^{a,b}, J. T. Olesberg^{b,c}, C. Cao^{a,b}, S. Veerasamy^{a,b},
M.E. Flatté^{a,b}, E. Koerperick^{a,b}, and T. F. Boggess^{a,b}, M. R. Santilli^d, and L.J. Olafsen^d

^aDepartment of Physics and Astronomy, University of Iowa, Iowa City, IA, USA 52246

^bOptical Science and Technology Center, University of Iowa, Iowa City, IA, USA 52246

^cDepartment of Chemistry, University of Iowa, Iowa City, IA, USA 52246

^dDepartment of Physics and Astronomy, University of Kansas, Lawrence, KS, USA 66045-7582

ABSTRACT

A focal plane array detector sensitive from 2.0-2.5 μm and consisting of 32, 1.0 mm x 50 μm pixels, all functional, is demonstrated. Mean room-temperature R_0A is found to be 1.0 $\Omega\text{-cm}^2$, limited by sidewall leakage. The focal plane array is fabricated from an MBE-grown homojunction *p-i-n* GaInAsSb grown on an *n*-type GaSb substrate. Back-illumination geometry is compared to front-illumination geometry and is found to be favorable, particularly the improved responsivity (1.3 A/W at 2.35 μm corresponding to 68% quantum efficiency) due to reflection of light off the metal contact. Further, back-illumination is the most convenient geometry for mounting the array onto a compact blood glucose sensor because both contacts can be mounted on one side, while detector illumination occurs on the other.

Keywords: Focal plane array, GaInAsSb infrared detector, back-illumination, MBE growth, wet-etching, dry-etching

1. INTRODUCTION

There is a great deal of interest in near-infrared detectors for the 2.0-2.5 μm wavelength region for diverse applications from medical and environmental sensing to astronomy. We are particularly interested in detector focal plane arrays optimized for mounting onto an integrated optical sensor for blood glucose monitoring. Such a sensor would pass light from a spectrally broadband bright source such as an LED through interstitial fluid, a fluid found under the skin that has glucose levels correlating closely to those in the blood; spectrally resolve the light; and detect the different wavelengths in a focal plane array. Using MEMS techniques, such a sensor has the potential to be extremely compact.

To be useful, the optical probe must cover wavelengths at which glucose specific absorption features occur, but at the same time avoid wavelengths at which water absorption is high. Water can strongly attenuate optical probe transmission and degrade the S/N of the measurement. The 2.0-2.5 μm wavelength region, known as the combination region, satisfies both criteria. In addition to glucose, other complex molecules in the interstitial fluid matrix, such as lactate, also have absorption features in the combination spectral region. Fortunately, multivariate calibration algorithms have shown that glucose concentrations in the complex matrix can be very effectively extrapolated [1,2]. The key requirement for such models to work is optical measurements with a sufficiently high S/N ratio.

Thus for a blood glucose sensor, the focal plane array must have high S/N ratio over the 2.0-2.5 μm combination spectral region. Furthermore, if the sensor is to be implantable sub- or trans-cutaneously, it should operate at room temperature. For maximal convenience in mounting the focal plane array onto the compact sensor, the array should be fabricated in a back-illuminated geometry, so that all electrical contacts can be on one side of the detector, while illumination of the array occurs on the other side. Another advantage of back-illumination compared to a front-illumination geometry is that it allows flip-chip bonding. Flip-chip bonding has a number of advantages over more conventional wire-bonding, an advantage that grows as the number of pixels in the array increases. In particular, by flipping the chip onto a custom header, electrical connections can be made to all pixels at once rather than individually wire-bonding each pixel.

We have chosen the GaInAsSb quaternary material system to grow *p-i-n* homojunctions and fabricate them into focal plane arrays. The GaInAsSb quaternaries have direct bandgaps that can be varied continuously over the 2.0-2.5 μm wavelength region while at the same time keeping the structure lattice matched to GaSb substrates [3], as shown for example in Fig. 1. Lattice-matching is extremely important because it minimizes defects in the crystal. Defects act as carrier generation-recombination centers, generating dark current and limiting detector signal-to-noise. Another advantage of lattice-matching is that it leads to a high yield of functioning pixels in an array. Malfunctioning pixels are problematic in highly strained structures, such as extended-wave InGaAs on InP.

2. MBE GROWTH

A solid state molecular beam epitaxy system (MBE) (Veeco-Applied-Epi 930) was used for the growth of the device structures. Nonequilibrium growth techniques such as MBE allow growth of alloys further into the miscibility gap than equilibrium growth techniques [4] (see Fig. 1). Dual filament Sumo cells were used for the Group III sources and valved cracker cells for the Group V sources. Be and GaTe were used as *p* and *n* dopants respectively. At the substrate temperatures employed during this growth (450-490°C), the Group III elements have approximately unity sticking coefficient and the growth rate is determined by the total Group III flux (J_{III}) [5]. Initially the growth rates of GaSb and InSb were calibrated against Ga and In cell temperatures respectively using Reflection High Energy Electron Diffraction (RHEED) intensity oscillations under excess Group V flux. The Ga and In fluxes (J_{Ga}^C & J_{In}^C) were then identified to grow the desired GaInAsSb alloy composition and growth rate. In order to find J_{Sb}^C , the critical Sb flux required to grow the quaternary, the RHEED intensity oscillations of GaSb growth with $J_{Ga} = J_{Ga}^C + J_{In}^C$ were measured under systematically varying Sb flux, starting from Sb-rich conditions. As the Sb flux was reduced below a critical flux J_{Sb}^C , the growth turned from Sb-rich to Ga-rich accompanied by a sharp reduction in the specular spot intensity and a reduction in the growth rate. During the actual quaternary growth this Group V (Sb) deficiency was compensated with the addition of As flux to achieve stoichiometric growth. Using this strategy, the quaternaries were consistently grown with the (004) high resolution X-ray diffraction (HRXRD) peak within a few hundred arcseconds of the GaSb (004) peak. Thereafter, we made small adjustments in J_{As} and J_{Sb} to fine tune the lattice matching. Samples used in this study had lattice mismatch less than $\pm 5 \times 10^{-4}$. The composition of the quaternary was cross-checked by determining the room temperature band gap from a photoluminescence measurement. Figure 2 shows bright room temperature photoluminescence for lattice-matched structures with bandgaps ranging from 2.2-2.5 μm .

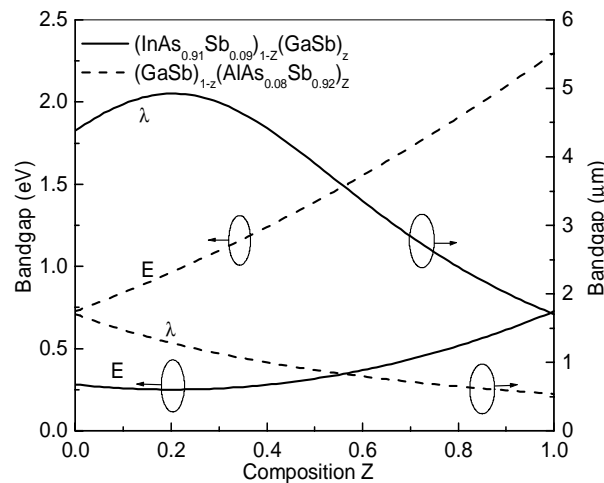


Fig. 1 Calculated bandgaps for GaInAsSb and AlGaAsSb quaternaries lattice matched to a GaSb substrate, from [6]. The miscibility gap prevents growth of alloys with midrange values of Z [7].

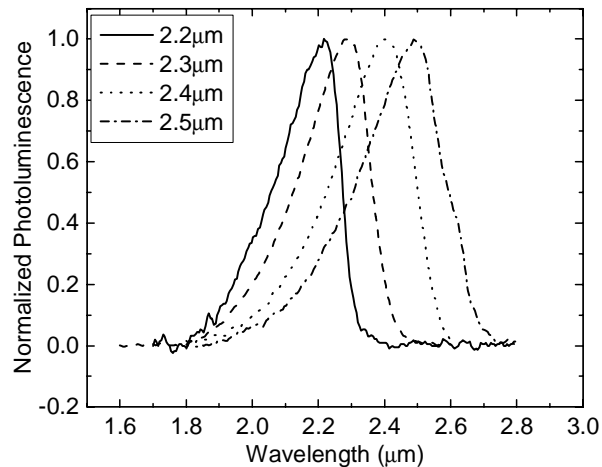


Fig. 2 Room temperature photoluminescence (PL) from GaInAsSb quaternaries lattice-matched to a GaSb substrate. PL samples consisted of nominally undoped GaInAsSb quaternary 0.4 μm thick with 50 nm GaSb cladding layers p -doped to $1 \times 10^{18} \text{ cm}^{-3}$ to avoid trapping of carriers at the heterointerfaces, which can suppress PL due to fast interface recombination velocities [8].

Figure 3 shows the device structures used for the front-illuminated (F-I) sample (IA1185) and the back-illuminated (B-I) sample (IA1209). We used a 500 μm , (100)-oriented n -type GaSb substrate doped to $1.9 \times 10^{17} \text{ cm}^{-3}$ for B-I detector as the substrate showed negligible optical loss in the wavelength region of interest (2.0-2.5 μm), as shown in Fig. 4. In contrast, 500 μm , (100)-oriented p -GaSb substrates doped to $1 \times 10^{18} \text{ cm}^{-3}$, used for the growth of F-I detectors, showed a very high optical loss due to free-carrier absorption, also shown in Fig. 4. For the F-I detector, p , i , and n layers were grown on a p -GaSb substrate. Incoming light then passed through the thin, lower-loss n -layer with less absorption. The active region is a 2 μm thick unintentionally p -doped GaInAsSb layer with a hole concentration of $1 \times 10^{16} \text{ cm}^{-3}$ and a mobility of $260 \text{ cm}^2 \text{ V}^{-1} \text{ s}^{-1}$. The surrounding p - and n -type GaInAsSb layers were doped to $1 \times 10^{18} \text{ cm}^{-3}$, and the n -layer was kept thin enough so that most of the radiation is absorbed in the 2 μm thick unintentionally doped active region. Doping levels were calibrated using a Hall setup in a Van der Pauw configuration. The substrate temperature during the growth was measured using an optical pyrometer. The substrates were slowly heated to approximately 510°C under Sb flux to desorb the oxide. Subsequently, the substrate temperature was brought down to 490°C for the growth of the doped GaSb buffer layer. All the subsequent layers were grown around 460°C. After the growth, the substrates were cooled slowly under As flux as the final layer is a 100 Å thick doped InAs contact layer. SCCM each and a RF power of 80 W resulting in a DC bias of 275 V at the substrate. The etch rate was about 70 nm per minute at room temperature. Subsequently, Ti/Pt/Au was deposited as a back metal contact on the F-I sample and Ni/AuGe/Ni/Au was deposited along the outer edge of B-I sample through a shadow mask, leaving most of the back surface uncovered for back illumination.

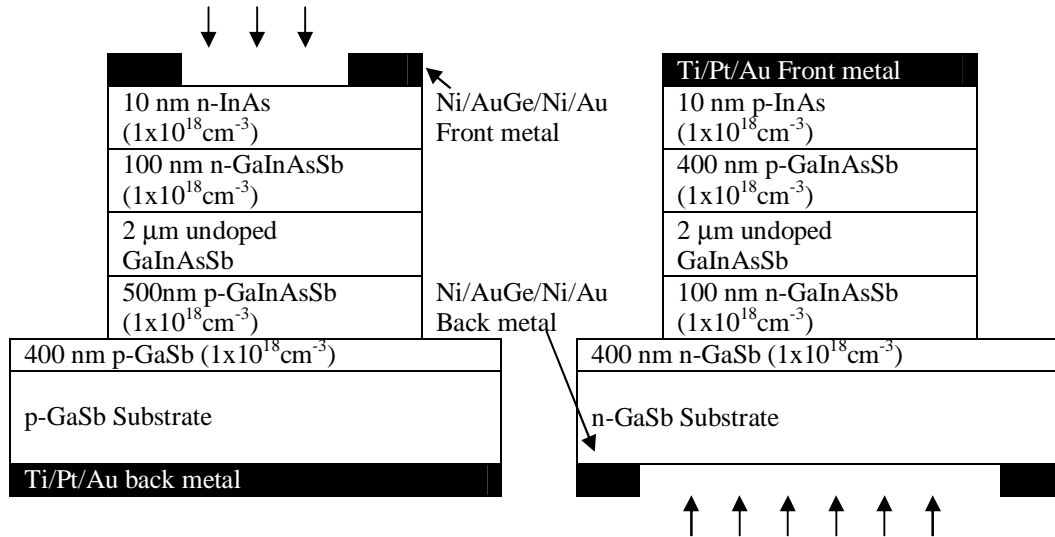


Fig. 3 Device structure for the front-illuminate (F-I) detector and the back-illuminate (B-I) detector. F-I detector has a circular mesa with diameter 410 μm and circular active area with a 200 μm diameter. The B-I device is a circular mesa with a 125 μm diameter.

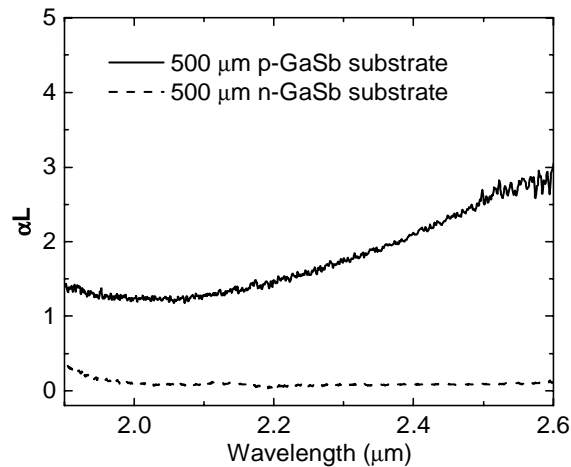


Fig. 4 Room temperature absorption coefficient α times thickness from a $L=500 \mu\text{m}$ thick, n - and p -type GaSb substrate doped to $1-9 \times 10^{17} \text{ cm}^{-3}$ and 10^{18} cm^{-3} , respectively. Absorption is very high in p -type GaSb substrates at these wavelengths due to free-carrier absorption, but is negligible for n -type substrates.

3. DEVICE PROCESSING

Device processing of the F-I (IA1185) and B-I (IA1209) structures was performed using dry-etching. The processing started with photolithography to define 125 μm diameter circular mesas on the B-I sample and ring patterns of 400 μm outer diameter and 200 μm inner diameter on the F-I sample as shown in Fig. 4. Ti/Pt/Au and Ni/AuGe/Ni/Au metals were deposited on B-I and F-I samples. Metal was lifted off the F-I sample to leave the ring metal contacts intact. A second lithography was carried out on the F-I sample to define the circular mesas of 410 μm diameter enclosing the ring contacts. A 120 nm thick layer of SrF_2 was deposited on both the samples as a dry etch mask, followed by the lift-off technique to remove the metal and SrF_2 from the unwanted places of the B-I sample and SrF_2 from that of the F-I sample. Reactive ion etching was used to etch the mesas down to the bottom heavily-doped GaSb epitaxial layer using a mixture of BCl_3 and Cl_2 . The etching was carried out at a system pressure of 5 mTorr, BCl_3 and Cl_2 flow rates of 5

SCCM each and a RF power of 80 W resulting in a DC bias of 275 V at the substrate. The etch rate was about 70 nm per minute at room temperature. Subsequently, Ti/Pt/Au was deposited as a back metal contact on the F-I sample and Ni/AuGe/Ni/Au was deposited along the outer edge of B-I sample through a shadow mask, leaving most of the back surface uncovered for back illumination.

Device processing of the focal plane array and of devices of variable size was done using wet etching on MBE-grown structures (IA1206, IA1187, respectively) nominally identical to the B-I detector shown in Fig. 4. Photolithography was used to define devices on the epi-side (*p*-side). Ti/Pt/Au (30 nm/50 nm/200 nm) contacts were deposited. The samples were etched for 60 min at room temperature in a citric acid:H₂O₂:H₃PO₄:deionized water blend at a concentration of 55:5:3:220, resulting in an etch depth of $3.7 \pm 0.1 \mu\text{m}$. The etch was uniform throughout the material and produced a smooth surface devoid of any defects that were not present prior to etching. After the etch, a shadow mask was used to cover the devices, and the same metallization was deposited to provide an *n*-contact on the epi-side.

4. DEVICE CHARACTERIZATION

The responsivity measurements of the GaInAsSb *p-i-n* devices were performed at room temperature with a Nicolet FTIR-Magna 56 spectrometer attached to a microscope. The responsivity of each detector mesa was spectrally resolved from 1.5-3.0 μm with an instrument bandpass of 2.5 nm. The responsivity of the detector was determined by normalizing the measured spectrum with that from a commercial InAs detector with a calibrated responsivity.

The I-V measurements of the detectors were measured using a Hewlett Packard 4155A semiconductor parameter analyzer. The device was placed backside-down on a gold-plated metal platform that was grounded via the analyzer, and a microprobe was used to connect to the contact on the top of each mesa.

5. RESULTS AND DISCUSSION

Figure 5 shows R_0A , the product of the room temperature differential resistance at zero bias and the detector area, an important figure of merit for detectors for a sampling of devices. The F-I device shows an R_0A of 0.96 ± 0.61 , and the B-I device shows an R_0A of 0.80 ± 0.18 . The slightly higher R_0A of the F-I sample can be explained by taking into consideration the dependence of the mesa diameter on sidewall leakage, as discussed below.

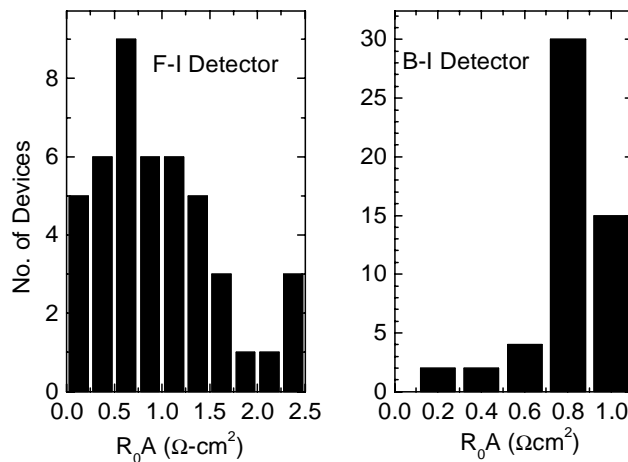


Fig. 5 Room temperature measurements of differential resistance at zero bias, R_0 , times detector area A for a sampling of front-illuminated (F-I) and back-illuminated (B-I) devices processed on wafers IA1185, and IA1209, respectively.

Figure 6 shows the dependence of room temperature R_0A on the perimeter-to-area ratio. The sample processed (IA1187) was nominally identical to the B-I sample (IA1209). The sample was wet etched, as described in Sec. 3, and all devices were processed on the same wafer on the same run. The plot shows that as the perimeter-to-area ratio

increases, R_0A decreases exponentially, indicating the increasing importance leakage current. The plot suggests that sidewall leakage current limits the R_0A , and that if the sidewalls could be passivated, much larger R_0A 's may be obtainable. However the small number of devices for smallest perimeter-to-area ratios do not make the data conclusive. In the future, more devices with smaller perimeter-to-area ratios should be measured.

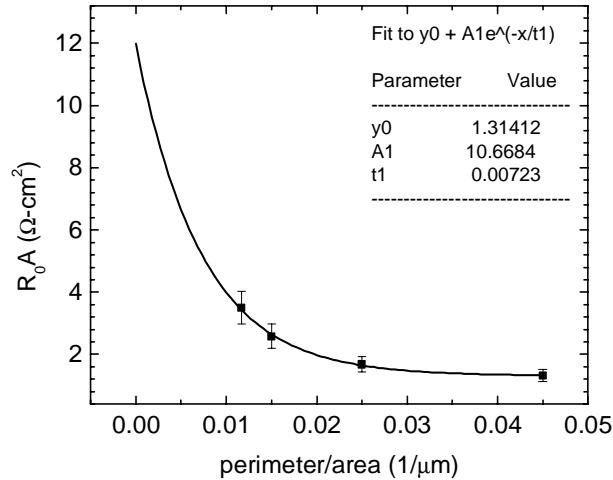


Fig. 6 The plot shows the dependence of R_0A on the separately wet-etched device mesa size (perimeter to area size). The points in order of increasing perimeter/area ratio represent the average of 1, 3, 11, and 10 devices, respectively. All devices were processed on the same wafer (IA1187) in the same processing run. Uncertainty bars represent standard deviation of the data, except for the smallest perimeter/area point: because the sample size was only 1, an uncertainty bar comparable in percent error to the other points was assigned.

Figure 7 shows the room temperature responsivity of some of the best B-I and F-I samples. The B-I device shows a square response of about 1.3 A/W across the 2.0-2.5 μm spectral region. The roll off below 2.0 μm is due to increasing absorption of the GaSb substrate. The dip in the response close to 2.5 μm is due to a water absorption peak. In contrast, the F-I sample shows a gradually increasing response for wavelengths shorter than 2.5 μm which peaks at about 2.0 μm at 1.0 A/W, then gradually rolls off for shorter frequencies. We observed a spread in the responsivity values of 0.78-1.30 A/W at 2.35 μm for B-I sample and 0.65-1.02 A/W at 2.0 μm for F-I sample. Maximum quantum efficiency of the B-I device is 68% at 2.35 μm , the maximum theoretical value with no anti-reflection coating. Maximum quantum efficiency of the F-I sample is 62% at 2.0 μm , and 41% at 2.35 μm .

The higher response of the B-I compared to the F-I, particularly at wavelengths close to 2.5 μm , is likely due to the influence of the metal contact. For the B-I device, the metal contact completely covers the mesa. Light that enters the backside of the device passes through the i-region. A portion of it is absorbed, and the remainder continues to the metal contact, where it is reflected, and makes a second pass through the i-region, increasing the device quantum efficiency, particularly at those wavelengths where absorption is low, i.e. near the 2.5 μm bandedge. In contrast, for the F-I device, light passes through the center of the ring contact and gets partially absorbed by the i-region. What gets transmitted through the i-region simply gets absorbed in the p-doped GaSb substrate and the excitation is lost.

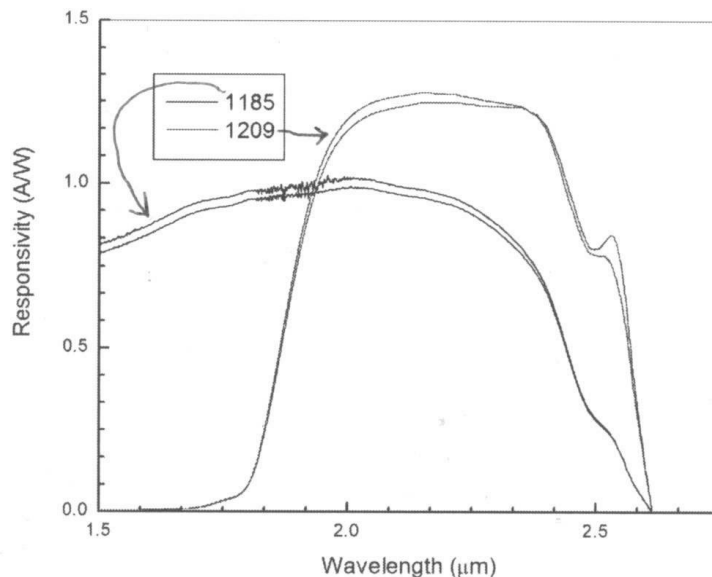


Fig. 7 Measured room temperature responsivity of some of the best B-I devices (IA1209) and F-I devices (IA1185).

Figure 8 shows a photograph of the contacts to the *p*-type layer (epi-side) of a focal plane array fabricated on a backside structure (IA1206) nominally identical to the B-I sample presented earlier. Not shown in the photo are the contacts to the *n*-type layer, on the same epi-side, and in a square around the perimeter of the pixels. Each of 32 pixels had dimensions of $50 \mu\text{m} \times 1.0 \text{mm}$, spaced by $10 \mu\text{m}$, and with a pad for wirebonding $100 \mu\text{m} \times 100 \mu\text{m}$. The array was processed using the wet-etching procedure described in Sec. 3. All pixels were found to be functional. A mean R_0A from two processing runs of $1.0 \Omega\text{-cm}^2$ was measured at room temperature, ranging from 0.3 to $4.2 \Omega\text{-cm}^2$ for a total of 15 pixels measured. The perimeter-to-surface ratio was 0.04; as suggested in Fig. 6, the R_0A of these pixels are likely limited by sidewall leakage.

Future improvements in processing should focus on eliminating sidewall leakage. Preliminary attempts at sidewall passivation during dry etching of mesas using different solutions, including sulfuric acid and 21% ammonium sulfide, produced no noticeable improvements in R_0A thus far, and in some cases degraded the responsivity. Other solutions and passivation steps should be explored. Alternatively, passivation with a dielectric coating should be explored, which should have the additional advantage of improving the long term robustness of the devices. For example, it was noted, though not carefully documented, that R_0A of both wet and dry etched structures with exposed sidewalls decreased on the scale of days to weeks. Another interesting alternative is to use ion implantation to define pixels. For example, a *n-i-i* structure is grown, then *p*-dopants are implanted into the top *i*-layer, followed by metallization. Sidewalls are then completely eliminated.

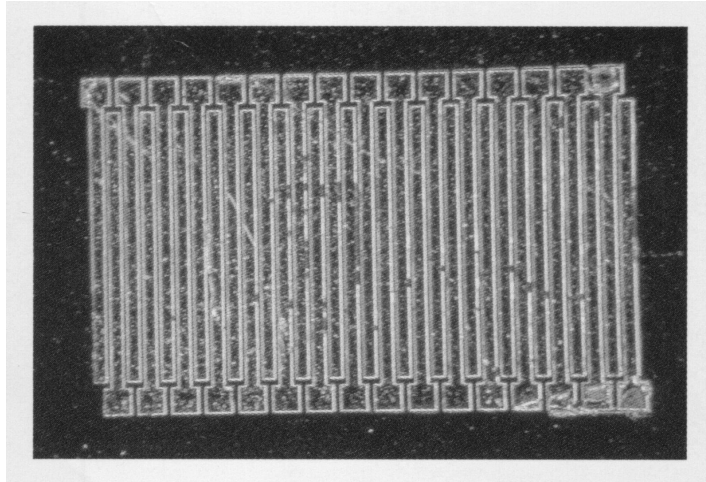


Fig. 8 A photograph of a 32 pixel array processed by wet etching on back-illuminated structure as discussed in Sec. 3. Shown in the photo are electrical contacts to the pixels (contacts on epi-side to p-type layer) with dimensions 1.0 mm x 50 μm , 10 μm space between pixels, and with 100 μm x 100 μm pads. Not shown in the photo are contacts on the same epi-side to the n-type layer. All pixels were found to be functional. R_0A was found to have mean 1.0 $\Omega\text{-cm}^2$.

In conclusion, we have grown and fabricated both F-I and B-I *p-i-n* homojunction GaInAsSb detectors, and found the performance of the B-I detectors favorable to F-I detectors, with a mean room temperature R_0A of 0.8 $\Omega\text{-cm}^2$, limited by sidewall leakage, and flat room temperature responsivities of 1.3 A/W (quantum efficiency 68% at 2.35 μm) across the 2.0-2.5 μm wavelength region. In particular, the B-I detectors have improved responsivities over the 2.0-2.5 μm wavelength region compared to F-I detectors due to the metal contact. B-I detectors are well suited to mounting on a compact, implantable blood glucose sensor because both contacts can be made on one side, while illumination of the detector occurs on the reverse side. B-I is also well suited for flip-chip mounting to a custom header, a useful feature for large arrays. A focal plane array consisting of 32 pixels, all functional, with dimensions 1.0 mm x 50 μm , 10 μm space between pixels, and pads of dimension 100 μm x 100 μm , and with room temperature $R_0A=1.0 \Omega\text{-cm}^2$ was demonstrated.

ACKNOWLEDGEMENT

All authors would like to acknowledge financial support for the work presented here from the NIH under contract #1R01DK64569-01.

6. REFERENCES

- [1] H. Chung, M.A. Arnold, M. Rhiel, D.W. Murhammer, "Simultaneous measurements of glucose glutamine, ammonia, lactate, and glutamate in aqueous solutions by near-infrared spectroscopy," *Appl. Spectrosc.* **50** (2), 270-76 (1996).
- [2] M.R. Riley, M.A. Arnold, D.W. Murhammer, "Effect of sample complexity on quantification of analytes in aqueous samples by near-infrared spectroscopy," *Appl. Spectrosc.* **54** (2), 255-261 (2000).
- [3] B.L. Carter, E. Shaw, J.T. Olesberg, W.K. Chan, T.C. Hasenberg, and M.E. Flatte, "High detectivity InGaAsSb pin infrared photodetector for blood glucose sensing," *Electron. Lett.* **36**, 1 (2000).
- [4] H. K. Choi, S. J. Eglash, and G. Turner, "Double-heterostructure diode lasers emitting at 3 μm with a metastable GaInAsSb active layer and AlGaAsSb cladding layers," *Appl. Phys. Lett.* **64**, 2474 (1994).
- [5] S.J. Eglash, H. K. Choi and G. W. Turner, "MBE growth of GaInAsSb/AlGaAsSb double heterostructures for infrared diode lasers," *J. of Cryst. Growth* **111**, 669-676 (1991).
- [6] I. Vurgaftman, J.R. Meyer, L.R. Ram-Mohan, "Band parameters for III-V compound semiconductors and their alloys," *Appl. Phys. Rev.* **89** (11), 5815-75 (2001).
- [7] M.P. Mikhailova and A.N. Titkov, "Type-II heterojunctions in the GaInAsSb/GaSb system," *Semicond. Sci. Technol.* **9**, 1279-1295 (1994).
- [8] D. Donetsky, S. Anikeev, G. Belenky, S. Luryi, C. A. Wang, and G. Nichols, "Reduction of interfacial recombination in GaInAsSb/GaSb double heterostructures," *Appl. Phys. Lett.* **81**, 4769 (2002).